A PORE NETWORK MODEL FOR CALCULATION OF INTERFACIAL VELOCITIES

H.F. Nordhaug [a], M. Celia [b], H.K. Dahle [a]

[a] *Department of Mathematics, University of Bergen, Johs. Brunsgt. 12, N-5008 Bergen, Norway*

[b] *Department of Civil and Environmental Engineering, Princeton University, Princeton, NJ 08544, USA*

Abstract

Two-phase flow in porous media is characterized by fluid-fluid interfaces that separate fluid phases at the pore scale. These interfaces support pressure differences between phases, and their dynamics lead to changes in phase saturation within the porous medium. Dynamic pore-scale network models mathematically track the dynamic position of each fluid-fluid interface through a pore network, based on imposed boundary conditions, fluid and solid properties, and geometric characteristics of the network. Because these models produce a detailed description of both phase and interface dynamics, results from these models can be volume-averaged to provide values for many macroscopic variables. These include traditional variables such as saturation and macroscopic capillary pressure, as well as non traditional variables such as amount of interfacial area in the averaging volume. With appropriate geometric definitions in the dynamic pore-scale model, a new algorithm may be included in the pore-scale network model to calculate a new variable: average interfacial velocity. This algorithm uses local information in any pore that contains a fluid-fluid interface to estimate the velocity of that interface over a time step. Summation over all interfaces in the network provides a measure of average velocity. Computations for dynamic drainage experiments indicate that this average interfacial velocity is well-defined and exhibits distinct behavior for stable and unstable displacements. Comparison of calculated interfacial velocities to a theoretical conjecture on the functional dependence of this macroscopic variable demonstrates another important use of pore-scale model, namely testing of new theories involving non traditional variables.

Key words: Two-phase flow, dynamic pore-scale network models, averaging, interfacial area, interfacial velocity, enhanced oil recovery

1. Introduction

Multi-phase porous media systems are characterized by fluid-fluid interfaces that exist at the pore scale. These interfaces define the spatial boundaries of each phase at any given instant in time. Interfaces also have properties such as interfacial tension, which allows each fluid to maintain a different pressure. The resulting difference between individual phase pressures is usually called capillary pressure. Fluid-fluid interfaces also provide the surfaces across which mass is transferred from one fluid phase to another, in problems such as dissolution of non aqueous phase liquid (NAPL) into flowing ground waters, evaporation of liquids into the gaseous phase, and exchange of dissolved components in hydrocarbon flooding and enhanced oil recovery. The amount of interfacial area present in a representative volume of porous medium controls the mass transfer process, while the spatial distribution of interfaces within the representative volume affects bulk properties of the fluid phases. While interfaces control many important properties of multi-phase systems, quantitative characterization of these interfaces has received relatively little attention in the porous media literature. Recent theoretical work of Gray and Hassanizadeh [1–3], and computational work of Miller and coworkers [4], Blunt and coworkers [5,6], Reeves, Held, and Celia [7–9], and Saripalli and coworkers [10,11], among others, have provided initial efforts to quantify bulk interfacial area, and to explore possible functional relationships between interfacial area, saturation, and capillary pressure. However, there has been very little work to quantify dynamical aspects of interfacial area.

In this paper, we present a model for interfacial area dynamics based on a pore-scale network approach. We use a dynamic pore-scale network model to describe interfacial dynamics at the pore scale, and use volume-averaging to compute averaged quantities to characterize interfacial area dynamics. To begin to provide a context for understanding

Email addresses: hansfn@mi.uib.no (H.F. Nordhaug), celia@princeton.edu (M. Celia), reshd@mi.uib.no (H.K. Dahle).

Article published in Advances in Water Resources 26 (2003) 1061–1074

and interpreting interfacial area dynamics, we use example calculations of interfacial quantities, and compare them to their counterparts computed for phase volumes. The pore-scale model we use is based on the original work of Blunt and King [12]. While Blunt and King focused on phase dynamics, we focus our calculations on interfacial dynamics. We choose this dynamic model because of its simplicity, and because it captures the essential features on which we choose to focus. We begin the presentation with a brief overview of pore-scale network models, then provide a detailed description of the model we have used. We next explain the averaging procedures used in our modeling, with a focus on averaged variables associated with interfacial areas, especially average interfacial velocity. We compare our results to laboratory measurements for interfacial area in a two-fluid system, [6], then provide computational results for interfacial area dynamics for both stable and unstable displacements. Finally, we compare our results to a simple theoretical conjecture relating interfacial velocity to fluid phase velocities, and conclude the paper with a discussion of the role of computational models and their relationship to new theoretical developments in the field of multiphase flow dynamics.

2. Pore-Scale Network Models

Pore-scale network models typically represent the pore space of the medium using simplified geometries, and within this geometric representation solve equations to track explicitly the location of all fluid-fluid interfaces within the network. Typical geometric representations include regular lattice structures, such as a cubic lattice, with pore bodies corresponding to the vertices of the lattice, and pore throats connecting the pore bodies. Pore bodies are often assigned spherical shapes, although cubes or other shapes with corners are sometimes used to account for wedge and corner flows. Similarly, pore throats may be cylindrical with circular cross section, or cylindrical with rectangular or perhaps triangular cross sections. For all of these choices, the geometry is kept sufficiently simple that interface configurations can be calculated analytically, for a given set of fluid pressures. These models are often run to mimic laboratory experiments, such as pressure cell tests to determine the relationship between capillary pressure and relative fluid saturation. This is accomplished by use of lattices that are sufficiently large to define meaningful continuum-scale measures, such as fluid saturation. Results of such simulations show all of the major features of experimental relationships, including finite entry pressures, residual saturations, and hysteresis. Because the simulators define interface geometries explicitly, additional geometric information may be extracted from network models. For example, fluid-fluid interfacial area can be calculated, given knowledge about the location and shape of each fluid-fluid interface.

Two general types of pore-scale network models may be identified: quasi-static models and dynamic models. In quasi-static models, the location of any fluid-fluid interface is governed by equilibrium considerations only. Equilibrium states are determined from the Young-Laplace equation, which relates the capillary pressure to the interfacial tension, the interface curvature, and local contact angle. For example, in simple cylindrical pores, the invasion capillary pressure for drainage is given by (see, for example, Dullien [13])

$$P_c^{\max} = \frac{2\sigma \cos\theta}{R} \tag{1}$$

In Equation (1), σ is interfacial tension, θ is contact angle, and R is the radius of the cylindrical pore throat. Other forms of this capillary equilibrium condition apply for different pore geometries. In a typical quasi-static pore-scale network model, a capillary pressure is imposed via boundary conditions on the network lattice, and each interface is tracked through the network with equilibrium positions determined by the stability test of Equation (1). If the interface is unstable, it is moved through the network until a stable position is found, or until it exits the network. No time dependence is included in the calculation; the interface is simply moved from one equilibrium position to another. This type of model is consistent with an algebraic relationship between capillary pressure and saturation, where changes in capillary pressure are translated instantaneously to changes in saturation. Examples of these kinds of models include those described in the books by Dullien [13], Sahimi [14], Ioaniddes and Chatzis [15], Hilpert and Miller [16], Ferrand and Celia [17], and Reeves [18], among many others. Models of this type are also used in other fields of science such as catalysis, see for example Hollewand and Gladden [19], and Rieckmann and Keil [20].

A second type of pore network model involves computation of transient behavior associated with interface movement. That is, unstable interfaces are tracked through the network until a stable position is reached, but the transient nature of the movement from one position to another is explicitly described and modeled. While these transient models are more computationally complex, they allow the underlying transients associated with interface movement to be incorporated and analyses explicitly. While most pore-scale network models reported in the literature are quasi-static, there have been several dynamic models that have been developed. These include the model of Blunt and King [12]; a series of models by Payatakes and coworkers [21–25], and more recent models by Mogensen and Stenby [26], Aker et al. [27], Dijkstra et al. [28] and by Dahle and Celia [29]. The models of Payatakes are the most comprehensive, including a focus on mobilization of trapped fluids and so-called drop traffic flows.

3. The dynamic network model

The pore-scale network model used herein is an extension of the model of Blunt and King [12]. We choose this model

because it incorporates interfacial dynamics, but is still sufficiently simple to allow for efficient calculations, and to allow us to isolate specific behaviors within the model. The pore network used in the model is a rectangular lattice having spherical pore bodies and cylindrical pore throats, with pore-size distributions defined for the bodies and throats, see Figure 2(a). Following Blunt and King [12], the model is simplified by the following assumptions: 1) local capillary pressure in the pore bodies is assumed to be negligible, so that only one pressure exists within a pore body, independent of the local saturation of that pore body (note that this does not mean that volume-averaged capillary pressure is zero); 2) while the radius of a pore throat, r_{ij}, serves to define its hydraulic conductance, the volume contributed by the pore throat is assumed to be small relative to volumes of pore bodies, therefore movement of an interface through a pore throat is assumed to occur instantaneously; 3) flow within pore throats is assumed to be laminar and given by Poiseuille's law; 4) both fluids are assumed to be incompressible. With these assumptions, the set of governing equations is relatively simple. Each fluid phase must obey volume conservation within each pore body, such that

$$V_i \frac{\partial S_i^\alpha}{\partial t} + \sum_{j \in N_i} Q_{ij}^\alpha = 0, \; i = 1, 2, ..., N \tag{2}$$

where N is the number of pore bodies, V_i represents the volume of pore body i, S_i^α represents local saturation (percent of V_i filled with fluid α), Q_{ij}^α is the volumetric flux from pore body i to it's neighbor j, and N_i is a list of all neighbor pore bodies for pore body i. This equation is written for both fluid phases, wetting ($\alpha = w$) and non-wetting ($\alpha = n$). The volumetric flux is related to pressures at the pore bodies by Poiseuille's law,

$$Q_{ij}^\alpha = G_{ij}^\alpha (p_i^\alpha - p_j^\alpha) \tag{3}$$

where p_l^α represents pressures, and G_{ij}^α represents hydraulic conductance in the pore throat connecting pore bodies i and j. Because the pore throats are cylindrical, and interface movement through them is instantaneous, only one fluid can occupy a given pore throat, at a given time. Therefore the fluid occupying the pore throat has conductance

$$G_{ij}^\alpha = \frac{\pi r_{ij}^4}{8 \mu^\alpha l_{ij}}, \tag{4}$$

while the non-occupying fluid has zero conductance. Summation of Equation (2) over the two phases gives the equation

$$\sum_{j \in N_i} (Q_{ij}^w + Q_{ij}^n) = 0 \tag{5}$$

Substitution of Equation (3) for each of the phase fluxes Q_{ij}^α provides a set of algebraic equations with the pore-body pressures as unknowns. These can be solved using standard matrix solution methods. Once the pressures are known, the fluxes are computed and saturations are updated as described below.

In the simulations reported herein, we only consider drainage, so that the resident fluid is the wetting fluid, and the invading fluid is non-wetting fluid. Time steps are chosen so that during any time step, only one pore body reaches full non-wetting phase saturation. That pore body then generates additional interfaces, located at all connecting pore throats that are filled with wetting fluid. Those interfaces are then tested for capillary stability, using the most recent pore body pressures and Equation (1). If the pressure drop Δp, over the pore throat exceeds the capillary pressure $P_c^{\max}$ of that pore throat ($\Delta p > P_c^{\max}$) as defined in Equation (1), then the interface associated with the pore throat is unstable. In that case it passes through the pore throat, non-wetting fluid occupies the pore throat, and non-wetting fluid can then begin to fill the adjoining pore body. If $\Delta p < P_c^{\max}$, the interface is stable and remains in place. Then the connecting pore throat is marked as trapped, with conductances set to zero for both phases.

Overall, the algorithm proceeds as an Implicit Pressure Explicit Saturation (IMPES) routine. The major unknowns are the pressure and saturation of each pore body. For a given distribution of fluids, phase conductances are calculated and put into Equation (5), which is solved for a new pressure field. That pressure field is then used in Equation (3) to compute fluxes through the pore throats. These fluxes are then used, in conjunction with knowledge of the current saturations in each pore body, to determine the minimum filling time for each of the pores, and this is set as the time step size. Then Equation (2) is used to update the saturations in each pore body. Newly created interfaces are tested for stability, conductances are updated, and the procedure is repeated. In the matrix solution for pressures, regions of wetting fluid that become completely surrounded by non-wetting fluid, and are therefore hydraulically trapped, are removed from the matrix equations to avoid singular matrices. This algorithm provides a transient response for both pressure and saturation. For any given time, knowledge of fluid occupancy and fluid pressure in all pore bodies allows volume-averaged variables to be computed.

In order to calculate volume-averaged variables, averages need to be defined over a representative volume. The volume may be chosen to correspond to the entire volume of the network, or it may be defined as essentially two-dimensional slices through the network, in the direction perpendicular to the macroscopic direction of displacement. In either case, volume-averaged saturation is defined as

$$S^\alpha = \frac{\sum_{i \in N_{vol}} V_i S_i^\alpha}{\sum_{i \in N_{vol}} V_i} = \frac{1}{V} \sum_{i \in N_{vol}} V_i S_i^\alpha \tag{6}$$

where V is the volume of the chosen averaging region, and N_{vol} denotes the set of pore bodies within the chosen averaging volume V. Macroscopic capillary pressure is defined as the difference between volume-averaged phase pressures, such that

$$P_c = p_n - p_w = \frac{\sum_{i \in N_{vol}} V_i S_i^n p_i}{\sum_{i \in N_{vol}} V_i S_i^n} - \frac{\sum_{i \in N_{vol}} V_i S_i^w p_i}{\sum_{i \in N_{vol}} V_i S_i^w} \tag{7}$$

where p_i corresponds to the pressure in pore body i. Notice that while no local capillary pressure exists (by assumption

in the model), a macroscopic capillary pressure is still well defined based on the average phase pressures.

Average properties associated with interfaces require somewhat more care in their definitions. Because no capillary pressure is associated with individual pore bodies, the shape (especially the curvature) of a particular interface is not specified. The only information for active (non-trapped) interfaces is that they reside in a specific pore body. To assign a measure of interfacial area, an interface within a filling pore body is assigned an area equal to the cross-sectional area of the pore throat pointing in the main direction of the flow (typically downwards in our simulations). Those interfaces trapped at the entrance to pore throats are assigned an area equal to the cross-sectional area of the pore throat. Therefore, the specific interfacial area, defined as the amount of interfacial area per unit volume of porous medium, is defined as

$$a^{wn} = \frac{1}{V}\Big(\sum_{i \in N_{vol}} a_i^{wn} + \sum_{j \in M_{vol}} a_j^{wn} \Big) = \frac{A^{wn}}{V} \qquad (8)$$

where M_{vol} denotes the set of pore throats that are contained within the averaging volume V.

Because we are interested in measures of macroscopic interfacial dynamics, we also wish to define a volume-averaged measure of interfacial velocity. This is the most difficult variable to define. Because the geometries of interfaces that reside within pore bodies are not resolved in detail within the pore body, their velocities need to be inferred from other variables. We use fluxes into and out of the pore body, changes in saturation within the pore body, and lengths of travel associated with the pore body and its connected pore throats to measure interfacial velocity. Consider a fluid-fluid interface that is created by complete filling of a given pore body. It first comes into contact with the connected pore throat, and a capillary stability test is performed. If the interface experiences sufficient capillary pressure to drive it through the pore throat, it will move through the throat with infinite velocity, then will fill the connected pore body at some finite rate, given by the subsequent computed changes in saturation for that pore body. The infinite speed is a consequence of the simplifying assumption that the pore throats are volumeless. To define a finite speed that preserves proper global velocities, the pore filling associated with saturation changes is extended in length to cover the combined pore body – pore throat combination, and the 'locally averaged' velocity for a specific interface is defined as

$$\|\mathbf{v}_i^{wn}\| = l_{i,j} \frac{\Delta S_i^n}{\Delta t} \qquad (9)$$

where the double brackets signify magnitude of the interface velocity vector, the length $l_{i,j}$ denotes the length of the pore throat through which the entering interface travels plus the diameter of the pore body i, and ΔS_i^n denotes the change in saturation over the time interval Δt. The direction assigned to the interfacial velocity vector is the average of the flow directions for the total inflow vector and total outflow vector for pore body i. Finally, the volume-averaged velocity vector is given by the sum of each interfacial velocity weighted by the area of the interface,

$$\mathbf{v}^{wn} = \frac{1}{A^{wn}} \sum_{i \in N_{vol}} \mathbf{v}_i^{wn} a_i^{wn} \qquad (10)$$

Volume-averaged phase velocities may be defined analogously, with volumes replacing areas as the appropriate weights, such that

$$\mathbf{v}^{\alpha} = \frac{1}{V S^{\alpha}} \sum_{i \in N_{vol}} \mathbf{v}_i^{\alpha} V_i S_i^{\alpha} \qquad (11)$$

where $\mathbf{v}_i^{\alpha}$ is given by an equation similar to Equation (9), with appropriate modification for the case of $S = 1$ or $S = 0$.

4. Equation testing and numerical results

In the following we use a three-dimensional pore network to compute averaged interfacial and phase velocities. We also compute other averaged variables, such as specific interfacial area, to demonstrate certain behavior patterns in the two-phase flow system. For the averaged quantities, we sometimes use a single averaging volume, spanning the entire network, and we sometimes use a 'sliding average' that involves slices of the total network volume. The latter averaging allows us to compute spatially varying averaged quantities.

A diagnostic tool for characterizing dynamic effects is the capillary number Ca. Following Lenormand et. al. [30], Ca is defined by

$$Ca = \frac{q\mu_{nw}}{A\sigma}, \qquad (12)$$

where q is the total flow-rate and A is the cross-sectional area of the network. Since the flow-rate q will vary throughout a simulation, we have tabulated the minimum and maximum values for the capillary number Ca. In our simulations,the values for Ca vary between 10^{-3} and 10^{-1}, see Table 1, which suggests that rate effects are important.

4.1. *Experimental setup*

All simulations are performed on a three-dimensional network of size $10 \times 10 \times 50$ pore bodies. When sliding averages are calculated, the size of the slices are $10 \times 10 \times 10$, and the averages as calculated along the largest direction (that is, the direction with 50 pore bodies, assumed to be the vertical direction). Experiments on network sizes up to $25 \times 25 \times 100$ have been performed. On a Linux-computer with 256MB RAM and a Celeron processor running at 470 Mhz, it took about 23 seconds to run a simulation on a $10 \times 10 \times 50$ network up to 50 time-steps, with a memory requirement of 4MB. The numbers for the larger network ($25 \times 25 \times 100$ nodes) were about 550 seconds and 43MB respectively. (The memory usage was measured, not calculated.) Since it takes one time-step to drain a pore body, it

follows that it takes less than 1/2 hour to drain the smaller network, whereas the larger network takes on the order of 100 hours to drain completely. The simulations on these networks showed the same qualitative behavior, and quantitative differences could mainly be attributed to the fact that the pore radii are chosen randomly. Thus, we feel confident that the chosen network size is appropriate for our initial investigations.

Boundary and initial conditions are set up to correspond to primary drainage. The top boundary is set to have a pressure of 4000 Pa, and fixed saturation of $S^w = 0$, while the bottom boundary is set with pressure of 0 Pa and saturation $S^w = 1$. No-flow conditions are imposed along the lateral sides of the domain. The initial condition is taken as $S^w = 1$, with a uniform pressure of 2000 Pa. This example is used to simulate the case where sufficiently large nonwetting phase pressure is imposed at the top boundary so that the network drains to residual saturation. We are interested in the transient response of the system to this pressure imposition. A range of pressure differences were tested and as long as the pressure was high enough to drain the network, the results were comparable. For example the amount of interfacial area did not vary more than 20 % among the different simulations.

We are interested in interfacial area dynamics for both stable and unstable displacements. A key parameter to be varied so that both stable and unstable displacements are simulated is the viscosity ratio M_μ defined by

$$M_\mu = \frac{\mu_{nw}}{\mu_w}, \tag{13}$$

While we have performed simulations over a range of viscosity values, we will use three representative values of viscosities so that the viscosity ratio M_μ =10, 1, and 0.1. Table 1 lists the viscosities, viscosity ratios, and the estimated capillary numbers for the selected experiments. In all simulations, the fluids are assigned an interfacial tension of 0.072 [N/m], and the contact angle is set at zero. We ignore density differences between the two fluids. The radii of the

Table 1
Dynamic parameters for selected experiments: Wetting and nonwetting fluid viscosities ([Ns/m^2]), viscosity ratios, total flows ([m/s]), and capillary numbers.

Set	μ_w	μ_{nw}	M_μ	$q_{\min}$	$q_{\max}$	$Ca_{\min}$	$Ca_{\max}$
1	0.001	0.010	10.0	$1 \cdot 10^{-2}$	$5 \cdot 10^{-2}$	$4 \cdot 10^{-2}$	$2 \cdot 10^{-1}$
2	0.001	0.001	1.0	$1 \cdot 10^{-2}$	$15 \cdot 10^{-2}$	$4 \cdot 10^{-3}$	$6 \cdot 10^{-2}$
3	0.001	0.0001	0.1	$5 \cdot 10^{-2}$	$20 \cdot 10^{-2}$	$2 \cdot 10^{-3}$	$8 \cdot 10^{-3}$

pore bodies and pore throats are generated using a cut-off log-normal distribution:

$$f(r;\sigma_{nd}) = \frac{\sqrt{2}\exp\left[-\frac{1}{2}\left(\frac{\ln\frac{r}{r_{ch}}}{\sigma_{nd}}\right)^2\right]}{\sqrt{\pi\sigma_{nd}^2}\, r\left[\operatorname{erf}\left(\frac{\ln\frac{r_{\max}}{r_{ch}}}{\sqrt{2\sigma_{nd}^2}}\right) - \operatorname{erf}\left(\frac{\ln\frac{r_{\min}}{r_{ch}}}{\sqrt{2\sigma_{nd}^2}}\right)\right]}.$$

The same standard deviation (σ_{nd}) is used for both the pore bodies and the pore throats, but different means (r_{ch}) and upper ($r_{\max}$) and lower ($r_{\min}$) cut-off values are used, see Table 2.

Table 2
Distribution parameters for pore and throat radius.

Standard deviation (σ_{nd})	0.25
Distance between pore body centers ($dx/dy/dz$)	$6.0 \cdot 10^{-3}$ [m]
Pore body mean (r_{ch})	$1.2 \cdot 10^{-3}$ [m]
Pore body lower cut-off ($r_{\min}$)	$0.6 \cdot 10^{-3}$ [m]
Pore body upper cut-off ($r_{\max}$)	$1.8 \cdot 10^{-3}$ [m]
Pore throat mean (r_{ch})	$4.0 \cdot 10^{-4}$ [m]
Pore throat lower cut-off ($r_{\min}$)	$2.0 \cdot 10^{-4}$ [m]
Pore throat upper cut-off ($r_{\max}$)	$6.0 \cdot 10^{-4}$ [m]
Estimated pore volume	$4.0 \cdot 10^{-5}$ [m^3]
Estimated cross-sectional area	$2.6 \cdot 10^{-5}$ [m^2]

4.2. *Validation of network model*

One of the objectives of this work is to use a computational pore-scale network model to investigate measures of average velocity of interfacial areas, and to compare those to analogous measures of average phase velocities. To our knowledge there are no experimental systems which gives data on average velocity of interfaces, although Magnetic Resonance Imaging (MRI) may potentially be used to give such data, see for example Johns and Gladden [31] for results in this direction. However, over the last decade several groups have provided data on interfacial areas, in particular related to research on NAPL, see for example [5,10,11,6] We have chosen to use experimental results obtained by Schaefer et.al. [6], as a validation experiment for our network code. In one of their experiments, a uniformly packed sand of cross-sectional area 5.1 cm^2 was initially completely water saturated. The porosity was estimated to be 42%, and the mean sand particle diameter was 0.335 mm. Approximately 20 ml of decane was then placed on top of the column, and the water was allowed to drain from the bottom. The surface tension was given to be 9 mN/m, and the viscosity of decane is approximately 0.93 10^{-3} Ns/m^2 at 300 K. In their their experiment, Schaefer et al [6] then measured the interfacial areas at different saturations.

From the data given in [6] a representation of the pore-space geometry was computed based on the monodisperse sphere packing model in [18]. Parameters for the distribution functions used in simulations are given in Table 3 leading to a porosity of approximately 35%. With these data we were able to give a fairly good fit to the experimental data in [6], as shown in Figure 1. By varying the mean pore throat radius about the estimate obtained from the sphere-pack model, we observed that the slope of the linear fits to the saturation-interfacial area curves varied like the inverse of the mean pore-throat radius. We also checked the sen-

sitivity with respect to the viscosity ratio, and found that the slopes of the linear fits changed by less than 10% when varying M_μ from 0.91 to 2, with $M_\mu = 0.91$ being the fit shown in Figure 1. A pressure drop of 800 Pa was used to drain the computational network model. Because no parameter adjustment was used, other than direct estimation of the pore size parameters (based on the sphere packing model), our model appears to give a reasonable description of the generation and transport of interfacial areas.

4.3. *Calculation of Local and Averaged Quantities*

Numerical solution of the network equations provides values for fluid pressures and associated saturations in each pore body, for each time step. From these values, and the geometry of both the network and the chosen averaging volumes, we compute averaged quantities as post-processing calculations. Because we have information about location and state of all fluid-fluid interfaces, we can distinguish between trapped and moving interfaces. Therefore, when defining averaged quantities, we may choose to distinguish between averages that include all interfaces, and averages that only involve active interfaces. As the default, we include all interfaces in the calculations, consistent with definitions such as that given in Equation (8). However, there are times when it may be useful to isolate only those interfaces that are moving. When averages are taken over active interfaces only, then we focus the calculations on pore bodies only, and we neglect pore throats, including pore throat volumes. The reason is that interfaces that are trapped will reside at the entrance to pore throats, so for consistency between interfacial discrimination and volume calculations, we decided to eliminate pore throat volumes and areas when we ignore trapped interfaces.

4.4. *Stable displacement*

Several simulations were run with viscosity rations greater than one. To illustrate the case of stable displacement, a viscosity ratio of 10 is used, with the boundary and initial conditions presented above. Network occupancy of fluids is shown in Figure 2(a), for an intermediate time corresponding to movement through the upper portion of the network. A flat, piston-like front can be seen moving through the network. Very little wetting fluid is left behind, with virtually all trapped wetting fluid existing as trapped singlets in pore throats. In Figure 2(b), average saturation, based on the sliding average concept given by Equation (6), is plotted as a function of depth. Since the dimension of the slices are $10 \times 10 \times 10$ nodes, the length scale of these averages are $10 \times dz$. Here, dz is the distance between pore body centers in the main flow direction given in Table 2. The macroscopic frontal behavior of the displacement is clear in this figure.

Average phase and interfaces velocities may be calculated for this case. In Figure 3, the average interfacial velocity is compared to the average phase velocities. Two different interfacial velocities are calculated, one that includes all interfaces and one that includes only active (that is, nontrapped) interfaces. We see that the curves are similar, although the interface velocity which include trapped interfaces is significantly less than the interface velocity calculated from active interfaces, as we would expect.

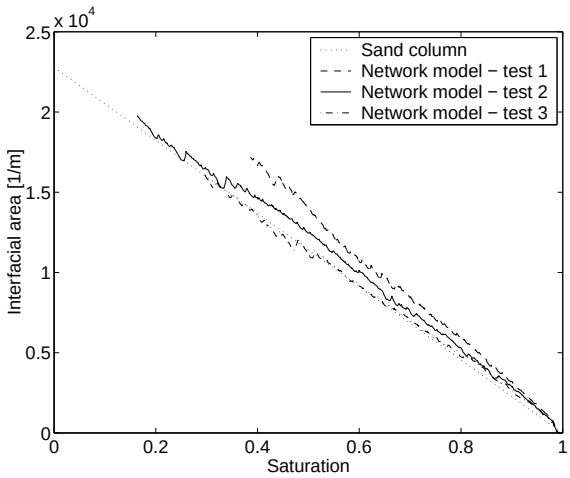

Fig. 1. Amount of interfacial area for sand column experiment,see [6], and network model.

4.5. *Unstable displacement*

To illustrate the model behavior in the case of unstable displacements, we use a viscosity ratio of 0.1, with the same boundary and initial conditions described above. In this case, we expect a much more irregular front, with possible viscous fingering, and this is essentially what we observe. In Figure 4(a), an irregular and fingered pattern is clear from the fluid occupancy plot of the network. The associated sliding average plot of average saturation as a function of depth (Figure 4(b)) shows a much more dispersed saturation distribution. Now when the average velocities are calculated, there is a very large disparity between average interfacial velocities and average phase velocities as shown in Figure 5. Furthermore, observe that the difference between the average interface velocity which includes trapped interfaces and interface velocity computed from active interfaces, is much larger than in the stable case (Figure 5(a)). We also see that the velocity of the nonwetting phase is very large compared to the wetting phase (Figure 5(a)). Both these effects are due to fingers of nonwetting fluid that rapidly penetrate the network.

To illustrate some additional difference between the stable and unstable displacements, we have plotted amount of interfacial area as a function of saturation for the viscosity ratios of 10, 1, and 0.1. Figure 6(a) shows the amount of trapped interfacial area as a function of saturation, with the most irregular fronts (viscosity ratio of 0.1) producing the largest amount of trapped interfacial area, and the most stable flat front (viscosity ratio of 10) producing the

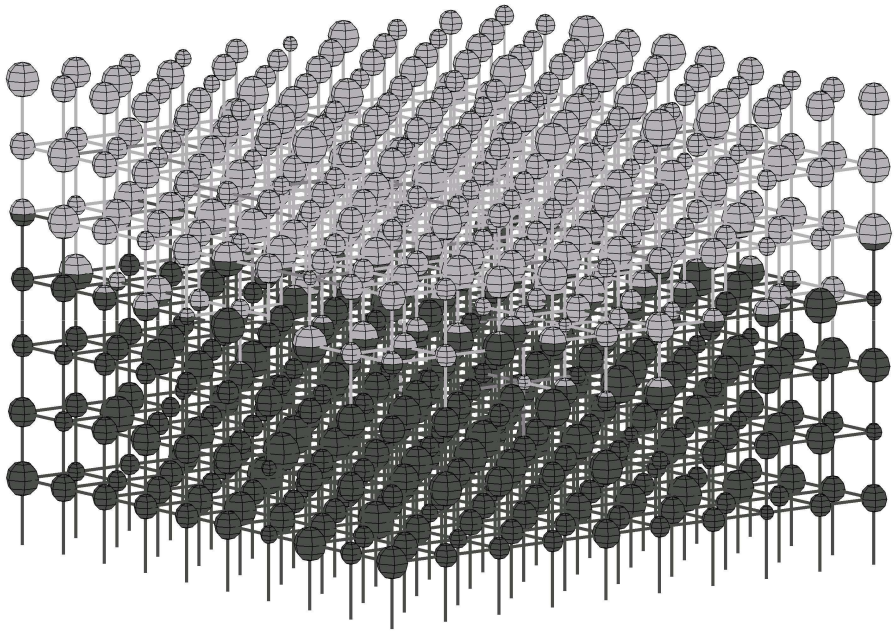

(a) microscale

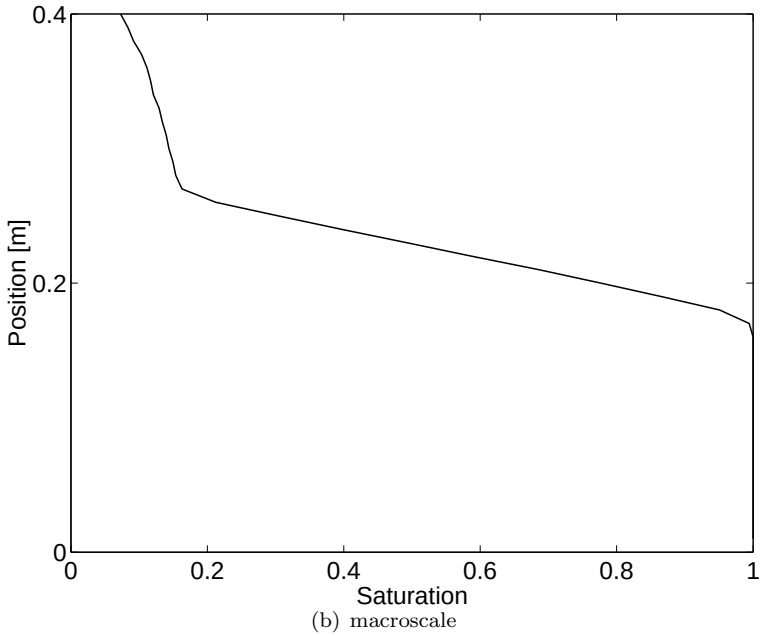

(b) macroscale

Fig. 2. Stable displacement – $M_\mu = 10.0$. Snapshot of the saturation front.

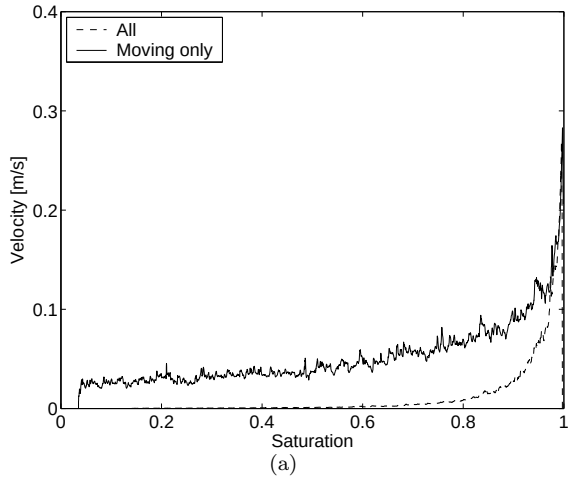

(a)

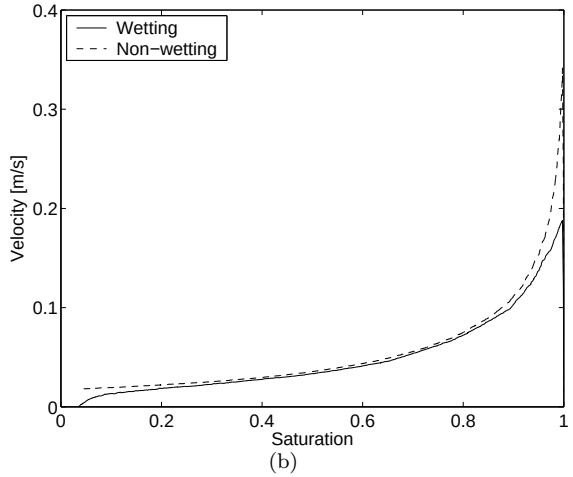

(b)

Fig. 3. Stable displacement – $M_\mu = 10.0$. Average interfacial velocity (a) and phase velocities (b). The averaging is over the entire network for each saturation.

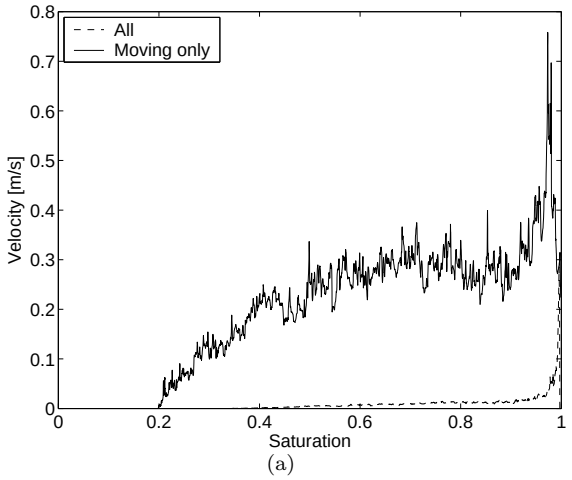

(a)

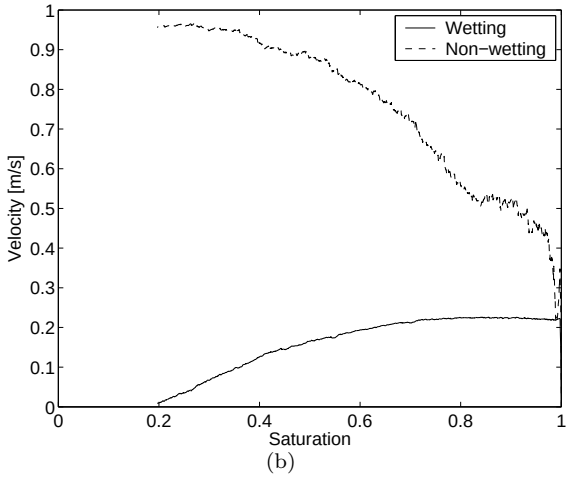

(b)

Fig. 5. Unstable displacement – $M_\mu = 0.1$. Average interfacial velocity (a) and phase velocities (b). The averaging is over the entire network for each saturation.

least amount of trapping. The clear trend is for increasing amounts of trapped interfacial area with decreasing viscosity ratio. This is a well known effect and to be expected from physical considerations.

In Figure 6(b), the amount of active interfacial area is plotted as a function of saturation, again for the three different viscosity ratios. Here we see a more complex relationship, but the unstable displacements clearly produce the largest amount of active interfacial area, but also produces the highest residual wetting phase saturation. The trend moves consistently to lower amounts of active interfacial area, and lower residual saturations, as viscosity ratio increases.

4.6. *Comparison to a Theoretical Conjecture*

One part of the recent theoretical work associated with Gray and Hassanizadeh has been an attempt to parameterize average interfacial velocity as a function of average phase velocities. One such attempt has been reported by Nordhaug et al. [32], who proposed the following relationship between volume-averaged interface velocity and volume-averaged phase velocities:

$$(\mathbf{R}^w_{wn} + \mathbf{R}^n_{wn}) \cdot \mathbf{v}^{wn} = \mathbf{R}^w_{wn} \cdot \mathbf{v}^w + \mathbf{R}^n_{wn} \mathbf{v}^n \tag{14}$$

In this equation, the coefficients $\mathbf{R}^\alpha_{wn}$ represent resistances to flow, and could be functions of phase saturation(s) or other variables. The general idea of the equation is that the interfacial velocity should be a weighted sum of the phase velocities. In the Appendix it is shown that under specific assumptions, Equation (14) can be reduced to the simple form

$$\mathbf{v}^{wn} = \frac{S^n \mathbf{v}^w + M_\mu S^w \mathbf{v}^n}{S^n + M_\mu S^w}, \tag{15}$$

where M_μ is the viscosity ratio.

While the resistance coefficients may be unknown, the general concept can be tested via a network model. In fact, because many of these variables cannot be measured experimentally at this time, the only tool available to test these proposed new equations is network simulations. To do this, we return to the computed velocities and compare calculated average interfacial velocities to those predicted by Equation (15). For the case of one-dimensional stable displacement reported earlier, the results in Figure 7(a) show

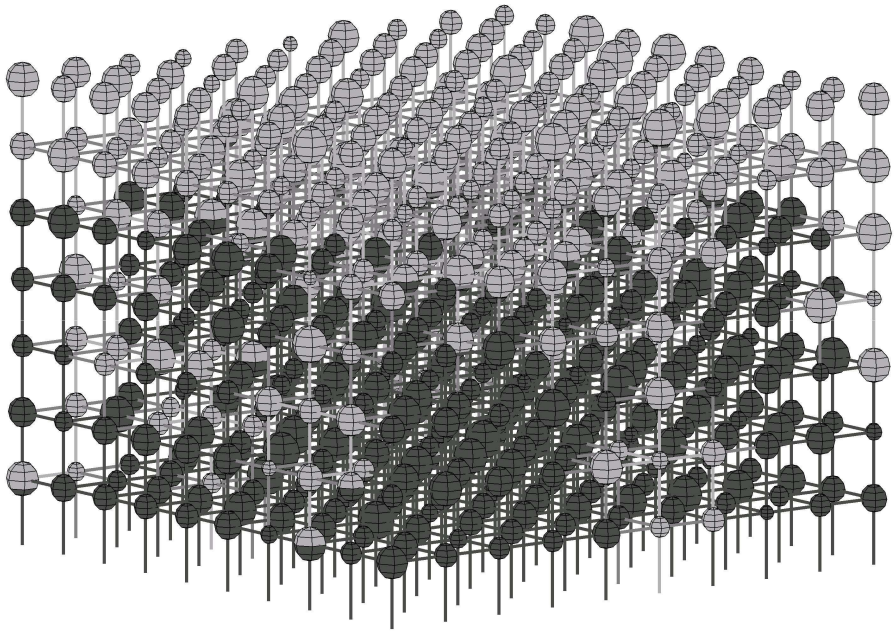

(a) microscale

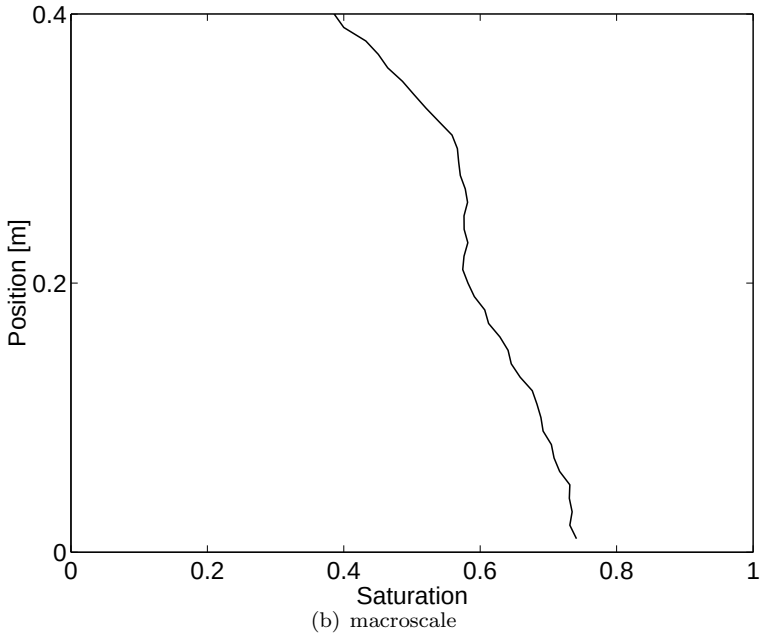

(b) macroscale

Fig. 4. Unstable displacement – $M_\mu = 0.1$. Snapshot of the saturation front.

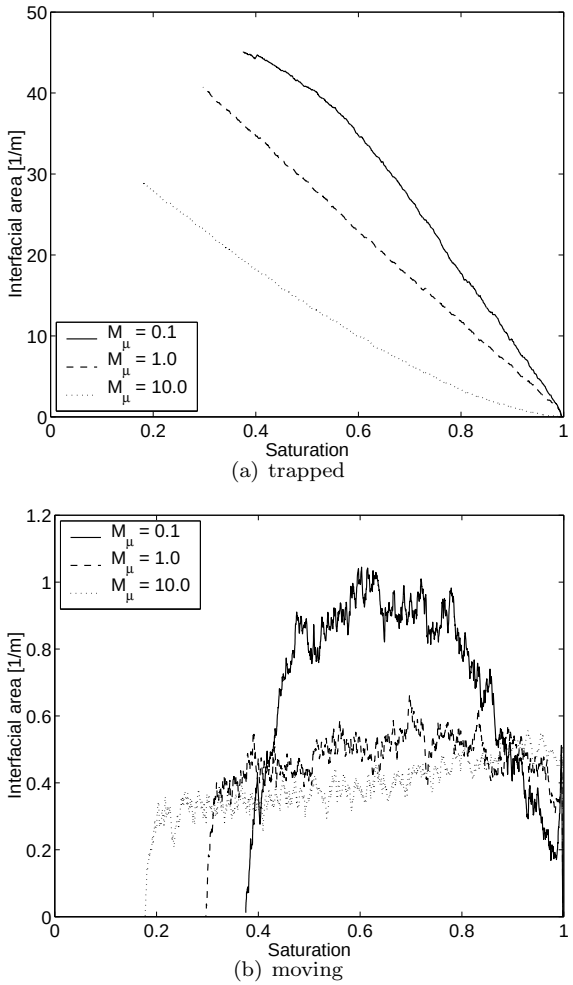

(a) trapped

(b) moving

Fig. 6. Amount of interfacial area for different viscosity ratios M_μ.

that the average interfacial velocity is consistently below the predicted values based on the average phase velocities (Equation (15)). A relatively poor prediction is also seen in the sliding averages shown in Figure 7(b). However, if we exclude the trapped interfaces, and only use active interfaces in the calculations, we find that the theory matches the numerical values quite well, see Figure 8. This is because elimination of trapped interfaces leaves only pores that are actively filling, and the macroscopically flat front means that interfaces are constrained to move with the same velocity of the invading and defending fluids, just as would happen in a single tube or pipe. So viscous stability, which produces a flat front macroscopically, leads to active interface velocities that are essentially identical to the two phase velocities, which themselves are equal. In this case, the theoretical equation appears to hold. However, inclusion of all interfaces leads to disparity between the values, due to the presence of trapped interfaces.

For the unstable case, we see consistently poorer predictions using the derived Equation (15). If the trapped interfaces are included in the calculation of the average interface velocity, Equation (15) completely fail to match the interfacial and the phase velocities as shown in Figure 9. A somewhat better match is obtained if only active interfaces are included in the interface velocity, see Figure 10.

Table 3
Distribution parameters for pore and throat radius in the validation experiment.

Standard deviation	0.10
Distance between pore body centers $(dx/dy/dz)$	$1.5 \cdot 10^{-4}$ [m]
Pore body mean - test 1	$5.0 \cdot 10^{-5}$ [m]
Pore body mean - test 2	$5.5 \cdot 10^{-5}$ [m]
Pore body mean - test 3	$6.0 \cdot 10^{-5}$ [m]
Pore body lower cut-off	$2.5 \cdot 10^{-5}$ [m]
Pore body upper cut-off	$7.5 \cdot 10^{-5}$ [m]
Pore throat mean	$4.0 \cdot 10^{-5}$ [m]
Pore throat lower cut-off	$2.0 \cdot 10^{-5}$ [m]
Pore throat upper cut-off	$6.0 \cdot 10^{-5}$ [m]
Estimated pore volume - test 1	$2.7 \cdot 10^{-9}$ [m^3]
Estimated cross-sectional area - test 1	$3.4 \cdot 10^{-9}$ [m^2]
Estimated pore volume - test 2	$3.6 \cdot 10^{-9}$ [m^3]
Estimated cross-sectional area - test 2	$2.7 \cdot 10^{-9}$ [m^2]
Estimated pore volume - test 3	$4.6 \cdot 10^{-9}$ [m^3]
Estimated cross-sectional area - test 3	$2.1 \cdot 10^{-9}$ [m^2]

We previously observed significant differences between interfacial and phase velocities, and these differences clearly result in the poor match between the interfacial velocities predicted by Equation (15) and those calculated in the network model. In the unstable case, local horizontal flows are more prevalent than in the stable case, due to the highly irregular shape of the invading front. However, the dominant flow direction remains the vertical. This essentially one-dimensional nature of the system is not sufficient to produce good matches between the theory and the calculations.

Overall, the proposed equation to relate average interfacial velocity to average phase velocities fails to capture this complex dynamics of interfacial movement. At present it seems like a more appropriate equation remains to be determined, perhaps by better exploiting the freedom in the choice of functional forms suggested in the Appendix.

5. Discussion

The dynamic network model presented herein uses a relatively simple algorithm at the pore scale to calculate phase and interface dynamics at the averaged, or porous-medium-continuum, scale. This model provides a systematic algorithm for calculation of new variables associated with fluid-fluid interfaces and their dynamics. Specifically, we calculate average interfacial areas as well as average interfacial velocities and examine their behavior under dynamic drainage for both stable and unstable displacements. While average interfacial velocities have not, to our knowledge, been measured in physical experiments, specific interfacial

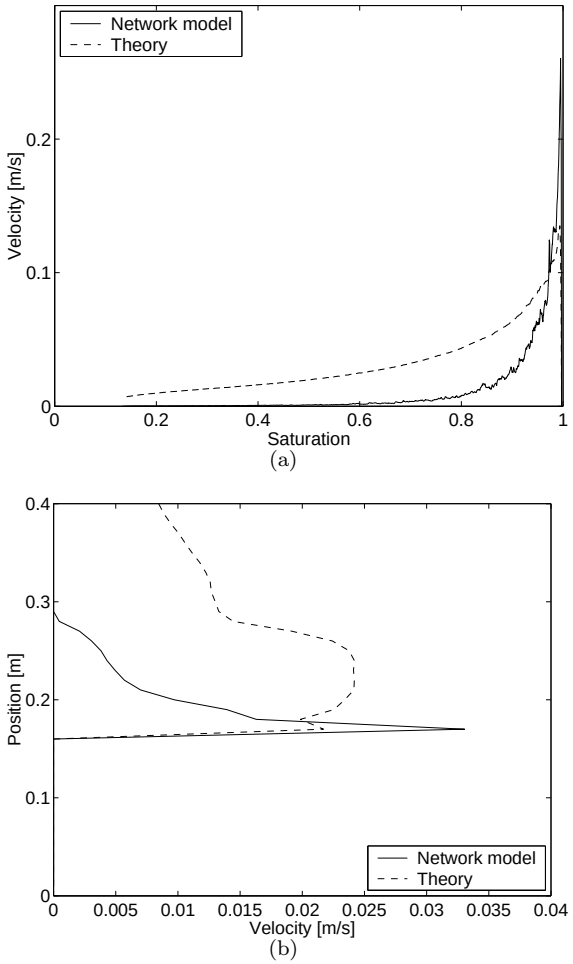

Fig. 7. Stable displacement – $M_\mu = 10.0$. Comparison of interface velocity in the network model and computed using phase velocities for one REV (a) and sliding REVs (b).

areas have been estimated in laboratory experiments. We use one reported measurement of interfacial area to test our model and find the predictions of interfacial area as a function of saturation to be very good over the entire range of measured saturations. While we recognize the lack of corner or wedge flows in our model, the good match to experimental data, with essentially no parameter fitting, provides confidence that this simple dynamic model captures essential physics in the system.

If macroscopic measures of interfacial area are to be included in the governing equations for porous media flows, as suggested by recent theoretical work [1–3], then governing equations for the dynamic evolution of interfacial area will need to be written. In these equations, variables like macroscopic interfacial velocity arise, and systematic quantification of these variables will be necessary. We provide herein the first computations, to our knowledge, of interfacial velocity, and provide initial evaluations of its behavior as a function of system dynamics. We also test a simple theoretical conjecture that relates macroscopic interfacial velocities to average phase velocities, and find that the proposed expression fails to capture the complexities of inter-

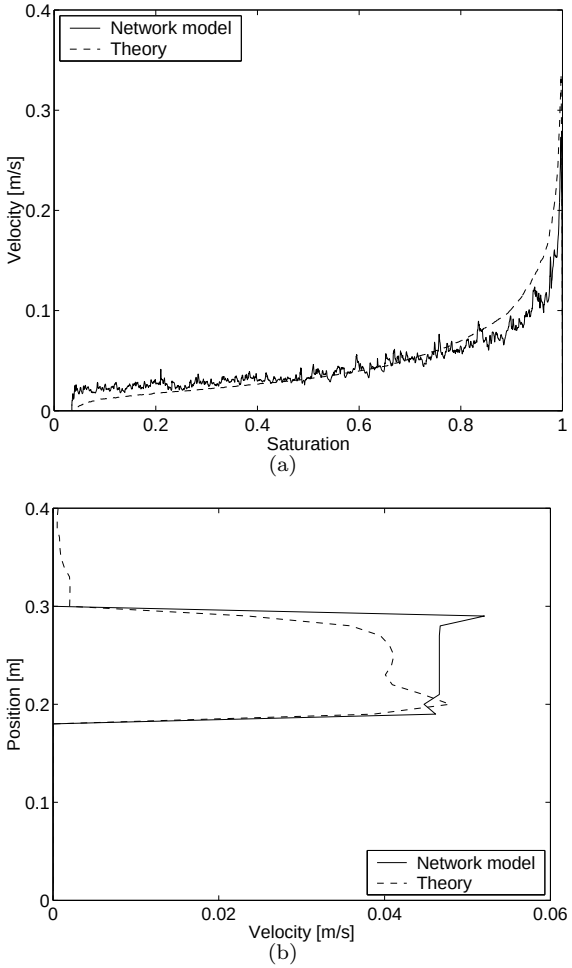

Fig. 8. Stable displacement – $M_\mu = 10.0$. Comparison of interface velocity in the network model and computed using phase velocities for one REV (a) and sliding REVs (b). Throat volume and trapped interfaces are not accounted for.

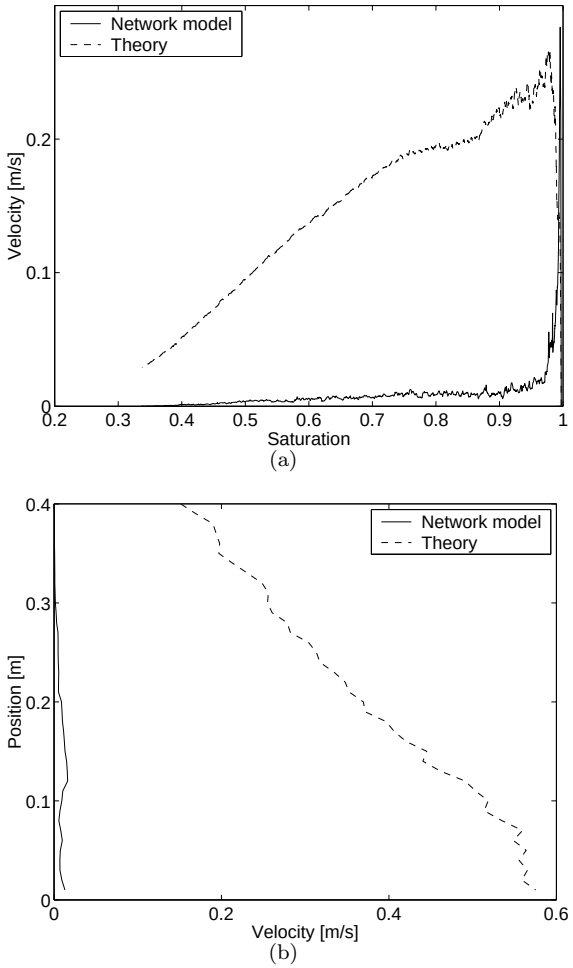

Fig. 9. Unstable displacement – $M_\mu = 0.1$. Comparison of interface velocity in the network model and computed using phase velocities for one REV (a) and sliding REVs (b).

facial dynamics. Additional theoretical development and analysis will be necessary to develop appropriate constitutive relationships involving fluid-fluid interfacial area and its dynamic evolution.

Overall we believe our model captures many of the essential features of two-phase flow in porous media. We also recognize that additional features should be included to make the systems more realistic. These include non-circular cross-sections for pore elements, so that corner and wedge flows may occur for the wetting phase. More complex shapes along the axial direction may also included, such as converging-diverging pore throats. Finally, inclusion of non-zero pore-throat volumes, with finite interfacial residence times in the pore throats, would also provide more realistic simulations. We are currently implementing these model enhancements. However, even with these enhancements, we expect to continue to use the general framework presented herein to calculate average interfacial velocities, and to use these velocities to examine new constitutive relationships and test new theories for multi-phase flow.

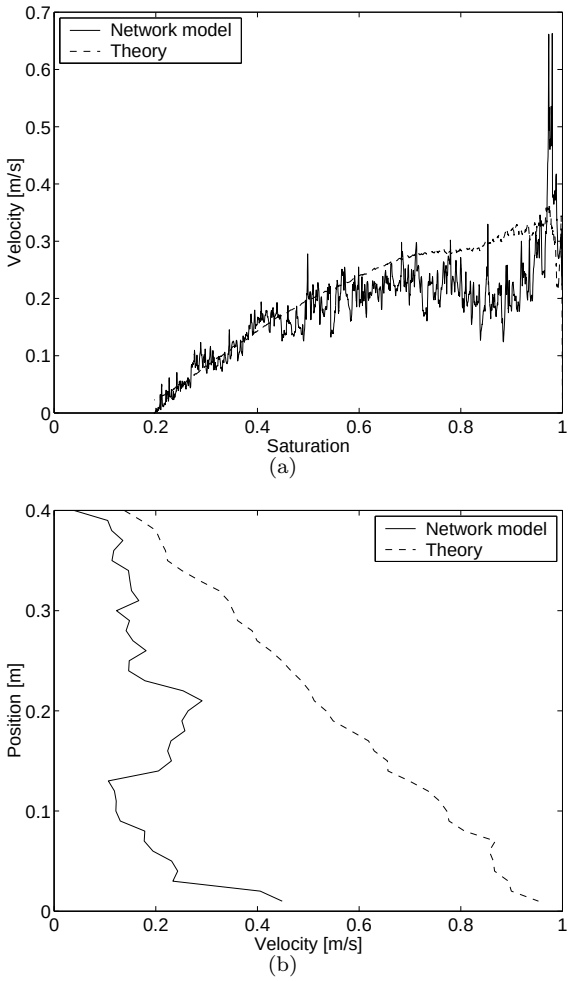

Fig. 10. Unstable displacement – $M_\mu = 0.1$. Comparison of interface velocity in the network model and computed using phase velocities for one REV (a) and sliding REVs (b). Throat volume and trapped interfaces are not accounted for.

Acknowledgments

The authors gratefully acknowledge the contributions of W.G. Gray and S.M. Hassanizadeh to this work. They also thank the anonymous reviewers for their useful comments and suggestions. Partial support for this work was provided to M.Celia by the National Science Foundation under Grant EAR-9805376 and to H.F. Nordhaug by the Norwegian Research Council (NFR) under grant 116153/431.

Appendix: Derivation of resistance terms $\mathbf{R}^{\alpha}_{wn}$

To illustrate the complexities introduced by interfacial area terms, a short derivation of Equation (15) is given here, showing the crude assumptions that are made. In [32] a complete model for two phase flow including interfacial area was presented. The governing equations include Equation (14) which represents momentum balance equations for a massless interface. In addition, we have mass-transport equation for phase α:

$$\frac{\partial(\varepsilon^{\alpha}\rho^{\alpha})}{\partial t} + \varepsilon^{\alpha}\rho^{\alpha}\nabla\cdot\mathbf{v}^{\alpha} = 0, \tag{16}$$

a generalized Darcy's law for phase α:

$$-\varepsilon^{\alpha}\nabla p^{\alpha} + \varepsilon^{\alpha}\rho^{\alpha}\mathbf{g} = (\mathbf{R}^{\alpha}_{wn} + \mathbf{R}^{\alpha}_{\alpha s})\cdot\mathbf{v}^{\alpha} - \mathbf{R}^{\alpha}_{wn}\cdot\mathbf{v}^{wn}, \tag{17}$$

and a transport equation for interfacial area written as:

$$\frac{\partial a^{wn}}{\partial t} + \nabla\cdot(\mathbf{G}^{wn}a^{wn}\mathbf{v}^{wn}) = F^{wn}. \tag{18}$$

Here $\epsilon^{\alpha} = \phi S^{\alpha}$ is the volume fraction of phase α with ϕ being the porosity, ρ^{α} is the density of phase α, $\mathbf{g}$ is the gravity, $\mathbf{G}^{wn}$ is a geometric tensor and F^{wn} refers to a general production term for interfacial area. In [32] the resistance terms $\mathbf{R}^{\alpha}_{wn}$ and $\mathbf{R}^{\alpha}_{\alpha s}$ in Equation (14) and (17) were assumed to take the form:

$$\begin{aligned}\mathbf{R}^{\alpha}_{wn} &= \mu^{\alpha}g^{\alpha}_{wn}(a^{wn})h^{\alpha}_{wn}(S^{\alpha})\mathbf{K}^{-1}{\varepsilon^{\alpha}}^{2},\\ \mathbf{R}^{\alpha}_{ws} &= \mu^{\alpha}g^{\alpha}_{\alpha s}(a^{ws})k^{-1}_{r\alpha}(S^{\alpha})\mathbf{K}^{-1}{\varepsilon^{\alpha}}^{2},\end{aligned} \tag{19}$$

where $\mathbf{K}$ and $k_{r\alpha}$ are respectively the absolute and relative permeabilities. These functional forms are chosen so that Equation (17) reduces to the usual Darcy law when effects of interfacial areas are neglected. It is also assumed that the dependencies on saturations and interfacial areas can be separated and the g- and h-functions must must be non-dimensional and positive. The volume fraction terms, ${\varepsilon^{\alpha}}^{2}$, are required to be able to go from average phase velocities to Darcy velocities.

When effects of interfacial area are negligible we should have that $g^{\alpha}_{\alpha s} = 1$ and $\mathbf{R}^{\alpha}_{wn} = 0$. Furthermore, in the limit that only one phase is present, say $S^{\alpha} = 1$, and the other phase vanish, say $S^{\beta} = 0$, we should have:

$$k_{r\alpha} = 1,\ \ k_{r\beta} = 0,\ \ \frac{a^{wn}}{a^{s}} = 0,\ \ \frac{a^{\alpha s}}{a^{s}} = 1,\quad \text{and}\ \ \frac{a^{\beta s}}{a^{s}} = 0.$$

In this case, since the interfacial area a^{wn} is zero, the resistance due to fluid-fluid interfaces $\mathbf{R}^{\alpha}_{wn}$ is also zero, and Equation (17) becomes

$$-\varepsilon^{\alpha}\nabla p^{\alpha} + \varepsilon^{\alpha}\rho^{\alpha}\mathbf{g} = \mathbf{R}^{\alpha}_{ws}\cdot\mathbf{v}^{\alpha},$$

with

$$\mathbf{R}^{\alpha}_{ws} = \mu^{\alpha}\mathbf{K}^{-1}{\varepsilon^{\alpha}}^{2},$$

Hence, we get that

$$g^{\alpha}_{wn}(0)h^{\alpha}_{wn}(1) = 0 \text{ and } g^{\alpha}_{\alpha s}(a_s) = 1. \tag{20}$$

The constraints obtained from the above considerations are far from sufficient to specify the resistance terms. In particular they give no information on the the tensor form of $\mathbf{R}^{\alpha}_{wn}$, which is conveniently assumed to be similar to $\mathbf{R}^{\alpha}_{\alpha s}$. One simple set of functions that satisfies the constraints imposed above are:

$$\begin{aligned}&g^{\alpha}_{wn}(a^{wn}) = \frac{a^{wn}}{a^{s}},\ h^{\alpha}_{wn}(S^{\alpha}) = (1-S^{\alpha})^{p}\\ &g^{\alpha}_{ws}(a^{ws}) = 1, \qquad k_{r\alpha}(S^{\alpha}) = (S^{\alpha})^{2}.\end{aligned} \tag{21}$$

If we assume that $\mathbf{K}$ is the identity matrix and substitute (19) and (21) into Equation (14), we obtain

$$\mathbf{v}^{wn} = \frac{(S^{n})^{p-2}\mathbf{v}^{w} + M_{\mu}(S^{w})^{p-2}\mathbf{v}^{n}}{(S^{n})^{p-2} + M_{\mu}(S^{w})^{p-2}}. \tag{22}$$

Since the interface velocity should be close to the non-wetting phase velocity when drainage starts and close to the wetting phase velocity when close to residual saturation, we have to chose $p > 2$. With $p = 3$ we obtain Equation (15).

References

[1] S. Hassanizadeh, W. Gray, Mechanics and thermodynamics of multiphase flow in porous media including interface boundaries, Adv. Wat. Res. 13 (4) (1990) 169–186.

[2] W. Gray, S. Hassanizadeh, Unsaturated flow theory including interfacial phenomena, Wat. Resour. Res. 27 (8) (1991) 1855–1863.

[3] W. Gray, S. Hassanizadeh, Macroscale continuum mechanics for multiphase porous-media flow including phases, interfaces contact lines, and common points, Adv. Wat. Res. 21 (4) (1998) 261–281.

[4] M. Lowry, C. Miller, Pore-scale modeling of non-wetting-phase residual in porous media, Wat. Resour. Res. 31 (1995) 455–473.

[5] L. Dillard, H. Essaid, M. Blunt, A functional relation for field-scale nonaqueous phase liquid dissolution developed using a pore network model, Journal of Contaminant Hydrology 48 (2001) 89–119.

[6] C. Schaefer, D. DiCarlo, M. Blunt, Determination of water-oil interfacial area during 3-phase gravity drainage in porous media, Journal of Colloid and Interface Science 221 (2000) 308–312.

[7] P. Reeves, M. Celia, A functional relationship between capillary pressure, saturation, and interfacial area as revealed by a pore-scale network model, Water Resources Research 32 (8) (1996) 2345–2358.

[8] R. Held, M. Celia, Modeling support of functional relationships between capillary pressure, saturation, interfacial area, and common lines, Adv. Wat. Res. 24 (3-4) (2001) 325–343.

[9] R. Held, M. Celia, Constitutive relationships derived from pore-scale network models, in: L. Bentley, J. Sykes, C. Brebbia, W. Gray, G. Pinder (Eds.), Computational Methods in Water Resources, Vol. 1, A.A Balkema, 2000, pp. 85–91.
[10] K. Saripalli, P. Rao, M. Annable, Determination of specific napl-water interfacial areas of residual napls in porous media using the interfacial tracers technique, Journal of Contaminant Hydrology 30 (1998) 375–391.
[11] K. Saripalli, H. Kim, P. Rao, M. Annable, Measurement of specific fluid-fluid interfacial areas of immiscible fluids in porous media, Environmental Science & Technology 31 (1997) 932–935.
[12] M. Blunt, P. King, Relative permeabilities from 2-dimensional and 3-dimensional pore-scale network modeling, Transport in porous media 6 (4) (1991) 407–433.
[13] F. Dullien, Porous Media: Fluid Transport and Pore Structure, 2nd Edition, Academic Press, 1992.
[14] M. Sahimi, Flow and Transport in Porous Media and Fractured Rock, VHC, Weinhim, Germany, 1995.
[15] M. A. Ioannidis, I. Chatzis, E. Sudicky, The effect of spatial correlations on the accessibility characteristics of 3-d cubic networks as related to drainage displacements in porous media, Wat. Resour. Res. 29 (1993) 1777–1785.
[16] M. Hilpert, C. T. Miller, Pore-morphology-based simulation of drainage in totally wetting porous media in porous media, Adv. Wat. Res. 24 (2001) 243–255.
[17] L. Ferrand, M. Celia, The effect of heterogeneity on the drainage capillary pressure - saturation relation, Wat. Resour. Res. 28 (3) (1992) 859–870.
[18] P. Reeves, The development of pore-scale network models for the simulation of capillary pressure - saturation - interfacial area - relative permeability relationships in multi-fluid porous media, Ph.D. thesis, Department of Civil Engineering and Operations Research, Princeton University (1997).
[19] M. P. Hollewand, L. F. Gladden, Modelling of diffusion and reaction in porous catalysts using a three-dimensional network model, Chem. Engn. Sci. 47 (1992) 1761–1770.
[20] C. Rieckmann, F. J. Keil, Multicomponent diffusion and reaction in three-dimensional networks: General kinetics, Ind. Eng. Chem. Res. 36 (1997) 3275–3281.
[21] M. Valavanides, A. Payatakes, True-to-mechanism model of steady-state two-phase flow in porous media, using decomposition into prototype flows, Adv. Wat. Res. 24 (3-4) (2001) 385–407.
[22] M. Dias, A. Payatakes, Network models for two-phase flow in porous media, Part 1. Immiscible microdisplacement of non-wetting fluids, Journal of Fluid Mechanics 164 (1986) 305–336.
[23] M. Dias, A. Payatakes, Network models for two-phase flow in porous media, Part 2. Motion of oil ganglia, Journal of Fluid Mechanics 164 (1986) 337–358.
[24] G. Constantinides, A. Payatakes, Network simulation of steady-state two-phase flow in consolidated porous media, AIChE J. 42 (2) (1996) 365–382.
[25] G. Constantinides, A. Payatakes, A theoretical model of collision coalescence of ganglia in porous media, J. Colloid Interface Sci. 141.
[26] K. Mogensen, E. Stenby, A dynamic two-phase pore-scale model for imbibition, Transport in Porous Media 32 (1998) 299–327.
[27] E. Aker, K. Maloy, A. Hansen, G. Batrouni, A two-dimensional network simulator for two-phase flow in porous media, Transport in Porous Media 32 (1998) 163–186.
[28] T. Dijkstra, G. Bartelds, J. Bruining, S. Hassanizadeh, Dynamic pore-scale network for two-phase flow, in: van Genuchten et al. (Ed.), Characterization and Measurement of the Hydraulic Properties of Unsaturated Soils, 1999, pp. 63–69.
[29] H. Dahle, M. Celia, A dynamic network model for two-phase immiscible flow, Comp. Geos. 3 (1999) 1–22.
[30] R. Lenormand, E. Touboul, C. Zarcone, Numerical models and experiments on immiscible displacements in porous media, Journal of Fluid Mechanics 189 (1988) 165–187.
[31] M. L. Johns, L. F. Gladden, Magnetic resonance imaging study of the dissolution kinetics of octanol in porous media, J. Colloid and Interface Science 210 (1999) 261–270.
[32] H. Nordhaug, H. Dahle, M. Espedal, W. Gray, M. Celia, Two phase flow including interfacial area as a variable, in: L. Bentley, J. Sykes, C. Brebbia, W. Gray, G. Pinder (Eds.), Computational Methods in Water Resources, Vol. 1, A.A Balkema, 2000, pp. 231–238.